Supporting Information

Experimental Section

1. Synthesis of CNT fibers.

The CNT fibers were produced by a continuous floating catalyst chemical vapor deposition method. Ferrocene and thiophene were used as the catalyst precursor and ethanol was used as the carbon source. The mixture liquid feedstock was injected into a vertical reactor kept at 1200 ^{o}C, and a mixture of Ar and H_2 was flowed across the vertical reactor. Then the CNT aerogel was continuously generated by coagulation of individual CNTs and pulled out of the reactor through a water coagulation bath for a contraction process to form continuous CNT fiber. The CNT fiber was then wound onto a spool outside of the reactor for use.

2. Preparation of CNT/MoO_3/PPy hybrid fiber.

The CNT/MoO_3 hybrid fiber was firstly prepared through an electro-deposition method. The MoO_3 electrodeposition solution was prepared by gently adding 30% aqueous hydrogen peroxide solution (v/v, 30%) into 1 g of molybdenum powder until the powder was completely dissolved, followed by diluting the solution to 50 mL with deionized water. In a typical electrodeposition process, the CNT fiber was used as the working electrode, and Pt foil and saturated calomel electrode were used as the counter and reference electrodes, respectively. The CNT fiber was first immerged in the MoO_3 electrodeposition solution for 5 min and then electrodeposited at a constant potential of -0.643 V (vs. SCE) for an electric quantity of 0.043 C·cm^{-1}. The product was then washed and heated at 80 ^{o}C in air for 1.5 h, followed by heating at 400 ^{o}C for 2 h in air to obtain the CNT/MoO_3 hybrid fiber. The CNT/MoO_3/PPy hybrid fiber was then prepared through an electro-polymerization process. The CNT/MoO_3 fiber was immerged in a solution containing 0.1 M pyrrole and 0.1 M KNO_3 at a pH of ~3 for 5 min and then the electropolymerization of pyrrole occurred at a constant potential of 0.7 V (vs. SCE) for an electric quantity of 0.67 C·cm^{-1}. The product was finally washed with deionized water and heated at 80 ^{o}C for 2 h in air to produce the CNT/MoO_3/PPy hybrid fiber.

3. Preparation of aligned CNT sheets.

Spinnable CNT array was firstly produced by a chemical vapor deposition method. Al_2O_3 (3 nm) and Fe (1.2 nm) were successively deposited on a silicon substrate as catalyst. Ethylene with a flowing rate of 90 sccm was used as the carbon precursor, and a mixture of Ar (400 sccm) and H_2 (30 sccm) was used as the carrier gases. The spinnable CNT array was obtained at 740 ^oC with a growing time of 10 min. Aligned CNT sheets were then continuously pulled out from the spinnable CNT array.

4. Preparation of CNT/NMO hybrid fiber.

$Na_{0.44}MnO_2$ was synthesized by grinding the mixtures of Na_2CO_3 and Mn_3O_4 (at a molar ratio of 1:1.377) for 1 h, followed by heating at 500 ^oC for 5 h at a heating rate of 5 $^oC \cdot min^{-1}$. The product was then cooled down and ground into powder, followed by heating at 900°C in air for 10 h at a heating rate of 5 $^oC \cdot min^{-1}$ to obtain NMO nanoparticles. 16 mg of NMO nanoparticles was dispersed in 20 mL of ethanol under probe-sonication at 200 W for 1 h to prepare NMO suspension with a concentration of 0.8 $mg \cdot mL^{-1}$. Five layers of aligned CNT sheets (2×15 cm) were stacked on a poly(tetrafluoroethylene) plate. The NMO suspension was dropped onto the CNT sheets on poly(tetrafluoroethylene) with the stacked CNT sheets fully immersed. The aligned CNT sheets were then twisted into a composite fiber by a spinning machine to produce the CNT/NMO hybrid fiber.

5. Fabrication of the fiber battery.

Chitosan solution was prepared by adding 0.9 g of chitosan into 20 mL acetic acid aqueous solution (2% by volume), followed by mechanical stirring for 2 h at 500 $r \cdot min^{-1}$. Poly(vinyl alcohol) (PVA) gel was prepared by dissolving 3 g of PVA in 17 g of deionized water for 2 h, followed by mechanical stirring at 95 ^oC for 1 h at 300 $r \cdot min^{-1}$. Then the chitosan solution and PVA gel were mixed together with a mass ratio of 1:1 to produce the chitosan/PVA gel. The CNT/NMO hybrid fiber was then coated with a layer of chitosan for prevention of short circuit of the fiber battery. The coating of chitosan was realized by dip-coating a CNT/NMO hybrid fiber into the chitosan/PVA gel, followed by heating at 80 ^oC for 30 min to obtain the chitosan-coated

CNT/NMO hybrid fiber. The CNT/MoO_3/PPy and chitosan-coated CNT/NMO hybrid fibers were finally twisted together to fabricate the fiber battery.

6. Injection of the fiber battery into the body.

The full injection process of fiber battery mainly included three steps. Firstly, the fiber battery was inserted into a syringe (with a size of one milliliter) containing normal saline (0.9% NaCl solution). For the convenience of injection, one end of the fiber battery was left outside the needle. Then the needle of the syringe was punched into the target region and the fiber battery was injected into the body. Finally, the needle of the syringe was pulled out of the body.

7. Electrochemical measurements.

For the convenience of electrochemical measurements, the electrodes of the fiber battery were extracted from the skin by CNT fibers. The galvanostatic charge-discharge, rate capability and cyclic performance of the fiber battery were measured with a two-electrode system using an Arbin electrochemical station (MSTAT-5 V/10 mA/16Ch). The galvanostatic charge-discharge curves, cyclic voltammetry (CV) curves, rate capability and cyclic performance of the hybrid fiber electrodes were measured with three-electrode systems through an electrochemical workstation (CHI 660a). To be specific, the hybrid fiber electrodes were firstly fixed on plastic plates and immersed in the oxygen-containing normal saline with a certain length. Then they were tested for galvanostatic charge-discharge and CV curves with saturated calomel and activated carbon electrodes as reference and counter electrodes, respectively.

8. Characterization and calculation.

The morphology of the fiber electrode was characterized by scanning electron microscope (SEM, JEOL JSM-6390). The photoacoustic images of battery-implanted tissues were collected and analyzed with a Vevo LAZR Imaging System (Fuji Film VisualSonics Inc). The photographs were taken by a camera (Nikon, J1). The internal stress was measured by compressing one end of the fiber (with a length of 4 mm) using a table-top universal testing instrument (HY-0350). The bending stiffness (D) was calculated from $D = EI$, where E and I are the elastic modulus and moment of inertia,

respectively. For a circular cross section with a diameter of d, the moment of inertia was calculated from $I = \pi d^4/64$. The modulus was measured with a bio-nanoindenter (Piuma Chiaro, Optics11, Amsterdam, The Neherlands). The specific capacity (C) of the injectable fiber battery was calculated from the equation of $C = (I \times \Delta t)/m$, where I, Δt, and m correspond to the discharge current, discharge time and weight of CNT/MoO_3/PPy hybrid fiber, respectively. The energy density of the injectable fiber battery was calculated from $E = (I \times U \times t)/v$, and the power density was obtained from $P = (I \times U)/v$, where I, U, t and v represent the discharge current, average operating voltage, discharge time, total volume of the injectable fiber battery, respectively.

9. Animals.

All animal experiments were conducted under a protocol approved by the Animal Experimentation Committee of Fudan University. Eight-week-old ICR white mice (female) were purchased from Shanghai SIPPR/BK Lab Animal Ltd. All the animals were treated according to the guidelines for the care and use of experimental animals described by the National Institutes of Health and Fudan University.

10. Biocompatible studies.

Biocompatibility tests were performed to verify the possible immune responses at the implantation site of the injectable fiber battery. The fiber batteries were firstly injected into the subcutis of mice for experimental group. 30 days after implantation, the subcutaneous tissues implanted with the fiber battery and the control group without implant were excised and incised into small pieces (about 1.5×1.5 cm^2) and fixed in a PBS solution with 4 wt% paraformaldehyde for 24 h. Next, H&E staining, F4/80 and LY-6G immunofluorescence staining were conducted according to the standard procedures. For histopathology analysis, 30 days after implantation, the hearts, livers, spleens, lungs and kidneys of the experimental and control groups were excised and fixed in 4 wt% paraformaldehyde for 24 h. H&E staining was then conducted according to a standard procedure for the histopathological evaluation. H&E staining and immunofluorescence staining slices were observed under microscope (Olympus BX51) and laser confocal microscope.

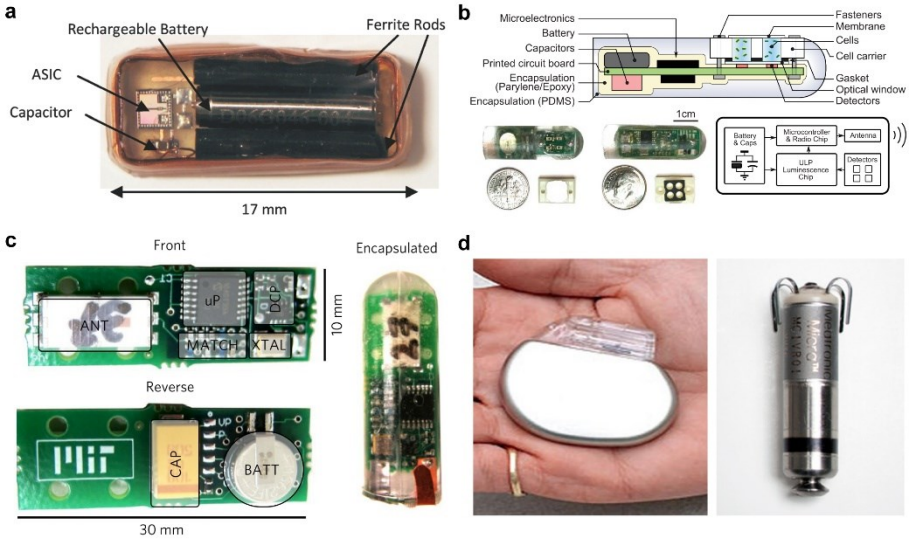

Figure S1. Different kinds of existing implanted conventional batteries. a, Implanted wirelessly charging battery system for bladder pressure monitoring[1]. **b**, The button-cell battery inside the capsule as power source for gastrointestinal health monitoring[2]. **c**, Energy-harvesting primary battery for continuous *in vivo* temperature sensing[3]. **d**, Commercial cardiac pacemaker (left) and its battery (right).

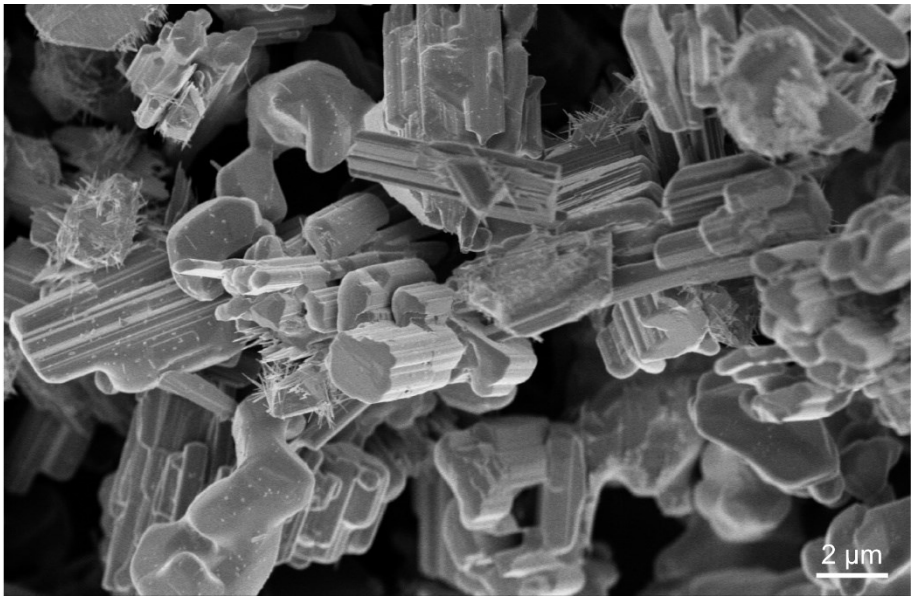

Figure S2. SEM image of NMO particles.

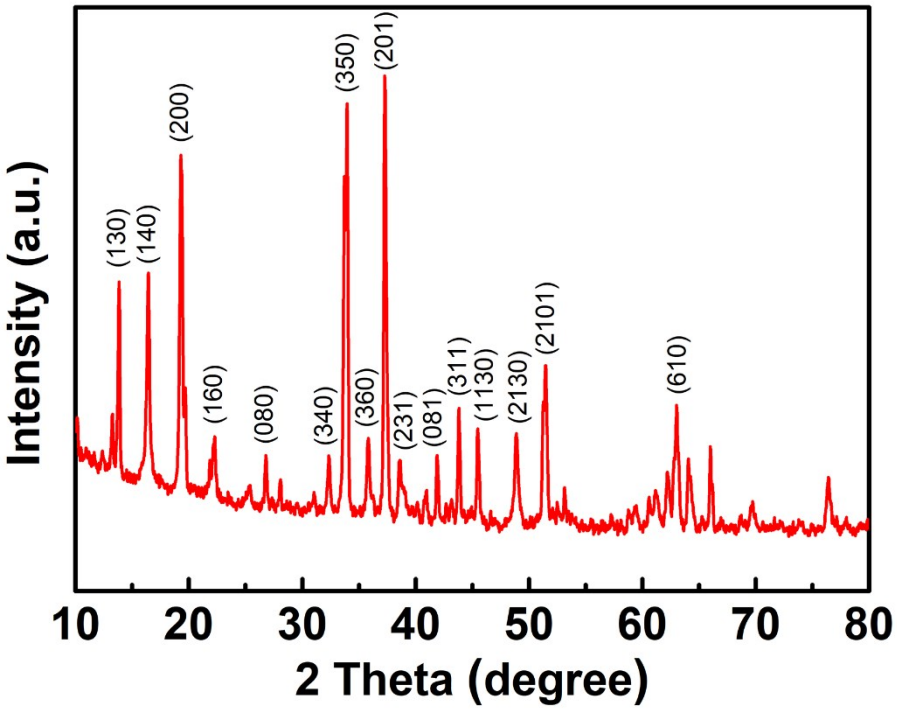

Figure S3. X-ray diffraction pattern of the NMO particles.

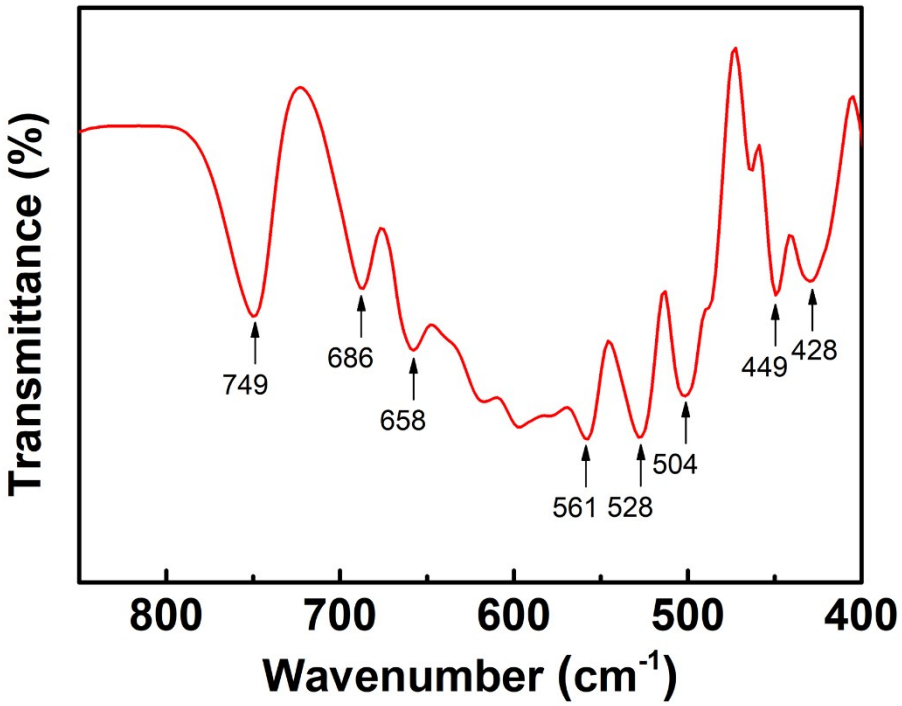

Figure S4. Fourier transform infrared spectra of the NMO particles.

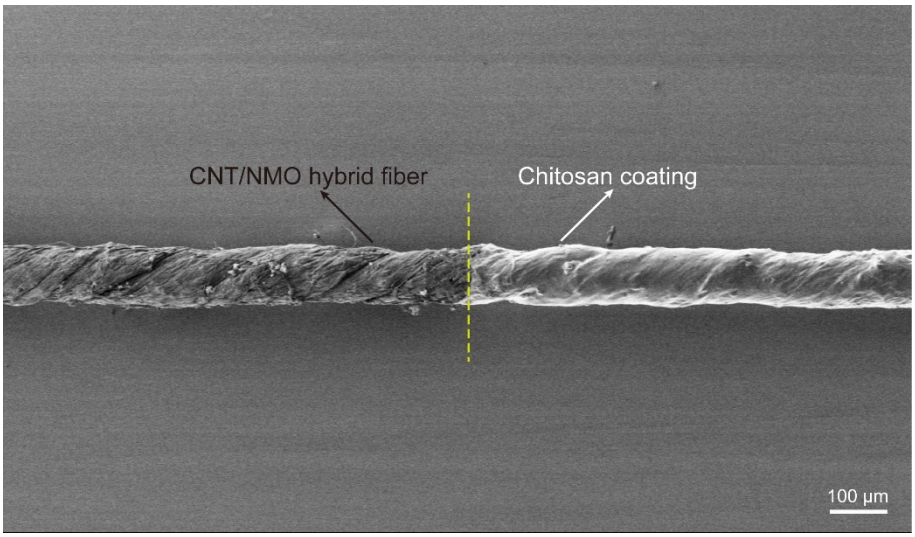

Figure S5. SEM image of the chitosan-coated CNT/NMO hybrid fiber.

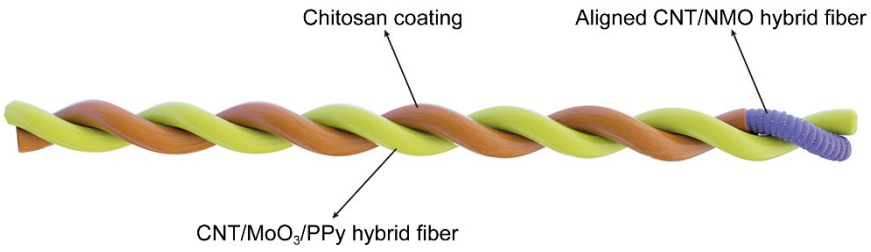

Figure S6. Schematic illustration to the structure of injectable fiber battery.

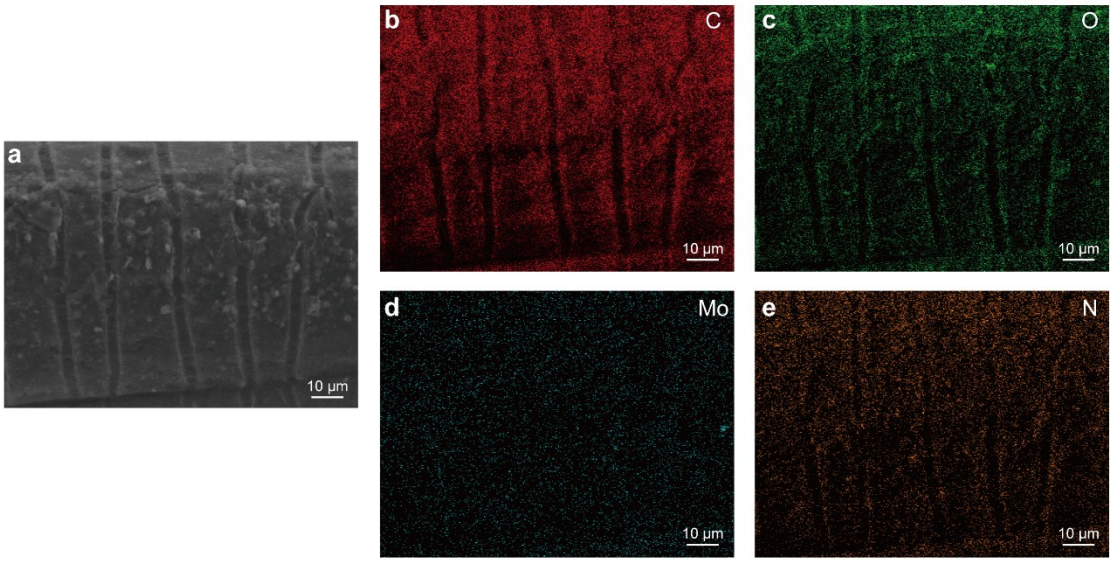

Figure S7. SEM image of the CNT/MoO_3/PPy hybrid fiber (**a**) and corresponding element mapping images (**b-e**).

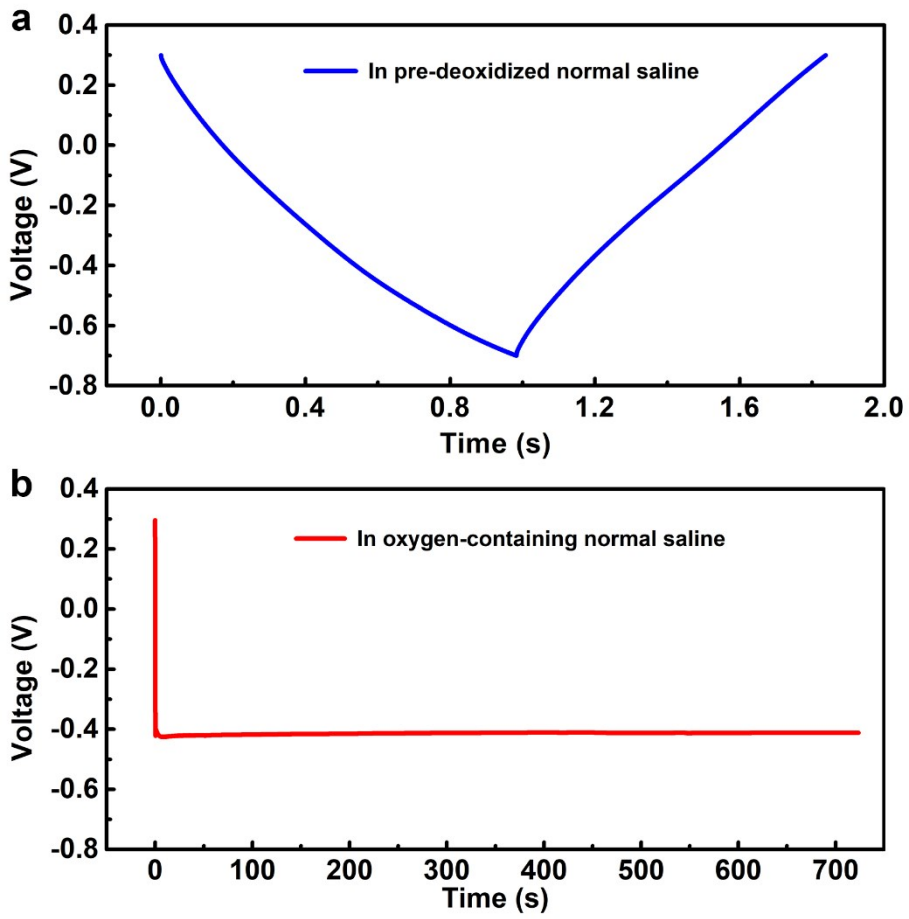

Figure S8. a, Galvanostatic discharge-charge curve of the CNT fiber electrode in pre-deoxidized normal saline at a current density of 1000 mA·g^{-1}. The CNT fiber electrode could be normally discharged to -0.7 V with little capacity in normal saline without O_2. **b**, Galvanostatic discharge curve of the CNT fiber electrode in oxygen-containing normal saline at a current density of 1000 mA·g^{-1}. The infinite discharge plateau at around -0.41 V was attributed to the side reaction of oxygen electrochemical reduction ($0.5O_2 + H_2O + 2\,e^- \rightarrow 2OH^-$).

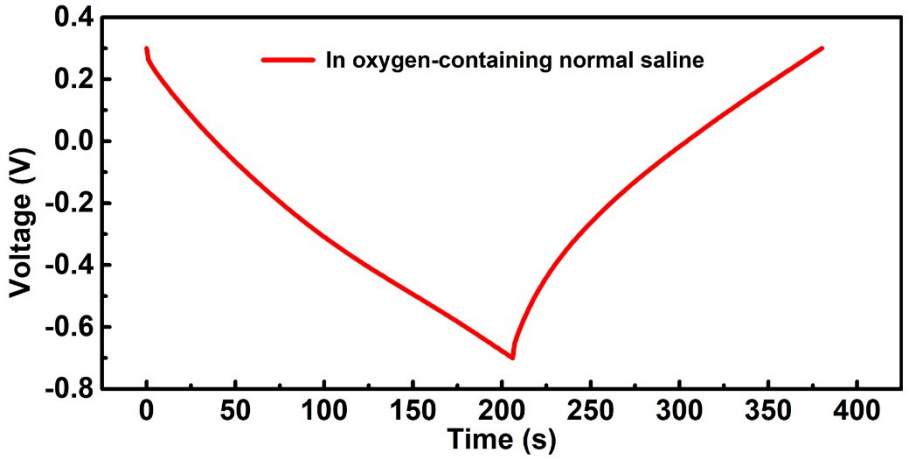

Figure S9. Galvanostatic discharge and charge curve of the CNT/MoO_3/PPy hybrid fiber electrode in oxygen-containing normal saline at a current density of 1000 $mA \cdot g^{-1}$.

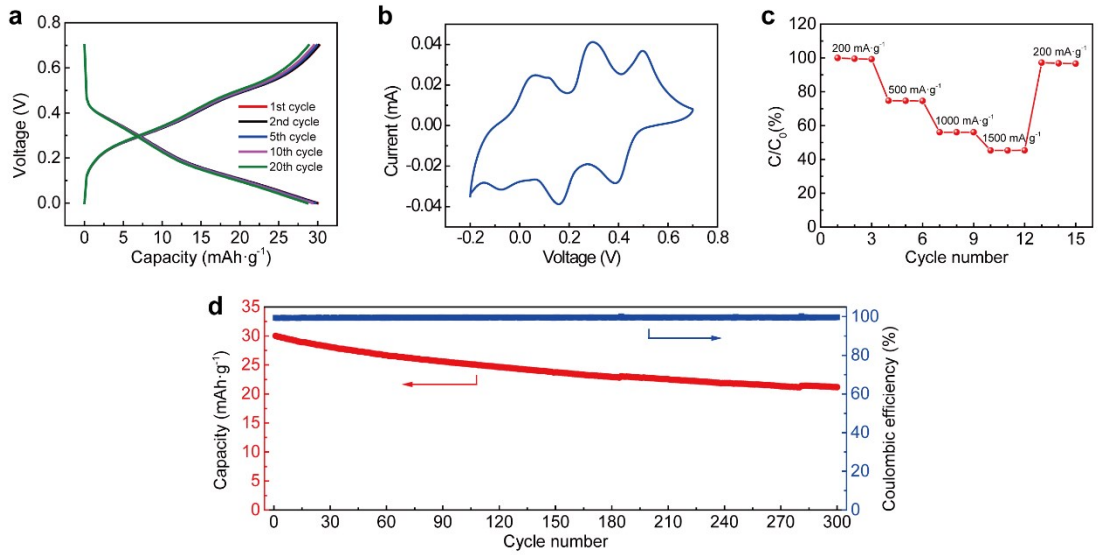

Figure S10. The *in vitro* electrochemical performance of the CNT/NMO hybrid fiber cathode in normal saline (0.9% NaCl solution). a, Galvanostatic charge-discharge curves of the CNT/NMO hybrid fiber at a current density of 1000 mA·g^{-1}. **b**, CV curve of CNT/NMO hybrid fiber in normal saline at a scan rate of 1 mV·s^{-1}. **c**, Capacity retention of CNT/NMO hybrid fiber when cycled at increasing current densities from 200 to 1500 mA·g^{-1}. **d**, Cyclic stability at current density of 1000 mA·g^{-1}.

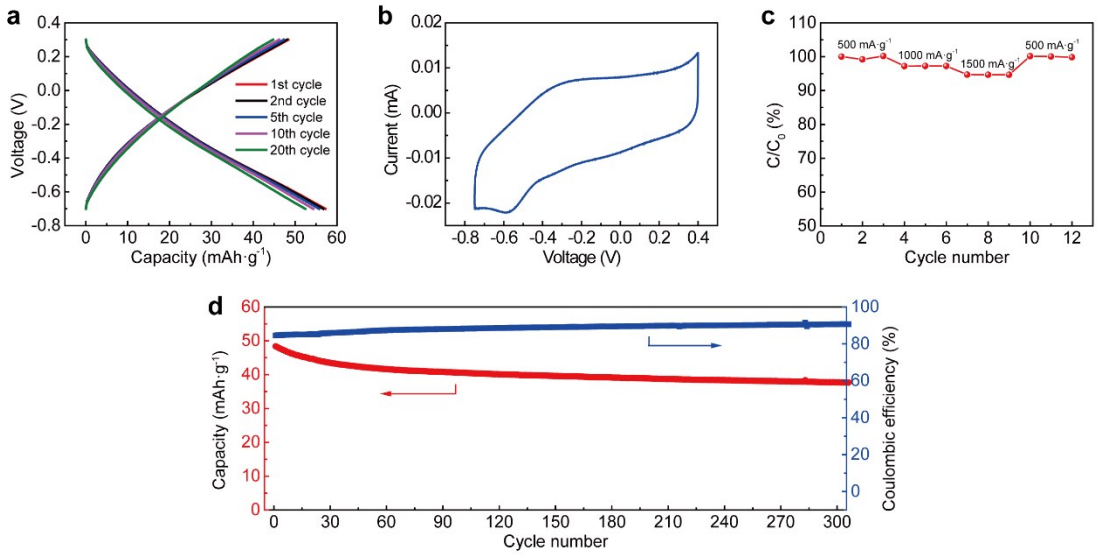

Figure S11. The *in vitro* electrochemical performance of the CNT/MoO_3/PPy hybrid fiber anode in normal saline. a, Galvanostatic charge-discharge curves of CNT/MoO_3/PPy hybrid fiber at a current density of 1000 mA·g^{-1}. **b**, CV curve of CNT/MoO_3/PPy hybrid fiber in normal saline at a scan rate of 1 mV·s^{-1}. **c**, Capacity retention of CNT/MoO_3/PPy hybrid fiber when cycled at increasing current densities from 500 to 1500 mA·g^{-1}. **d**, Cyclic stability at the current density of 1000 mA·g^{-1}.

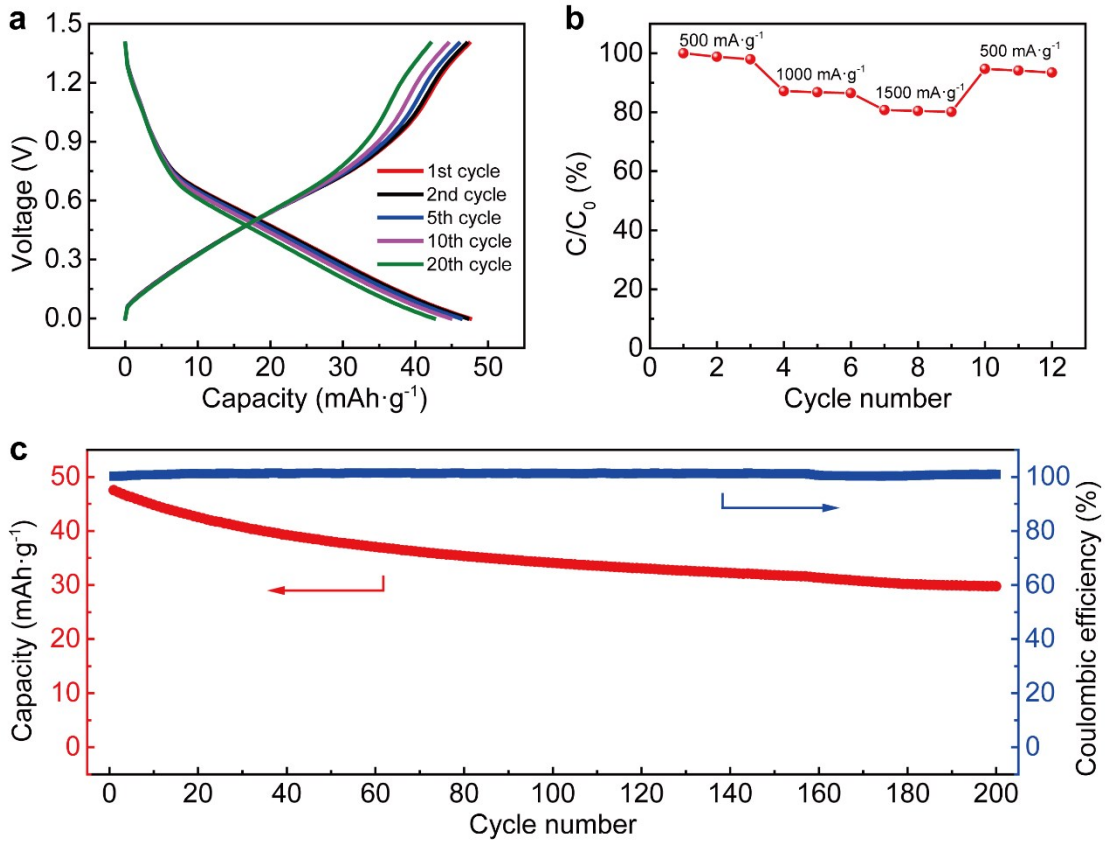

Figure S12. The *in vitro* electrochemical performance of the injectable fiber battery in normal saline. a, Galvanostatic charge-discharge curves of the fiber full battery at current density of 1000 mA·g^{-1}. **b**, Capacity retention of the fiber battery when cycled at increasing current densities from 500 to 1500 mA·g^{-1}. **c**, Cyclic stability at current density of 1000 mA·g^{-1}.

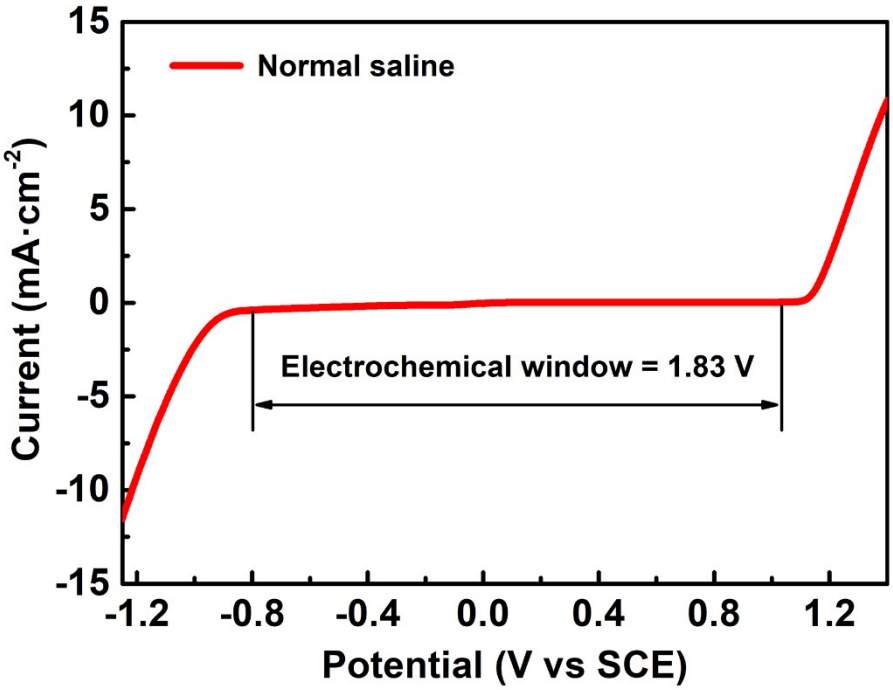

Figure S13. The electrochemical stability window of normal saline. The highest voltage of the fiber battery (1.4 V) was much lower than the electrochemical stability window of normal saline (1.83 V), which proved the stability and safety of the fiber battery during charging/discharging.

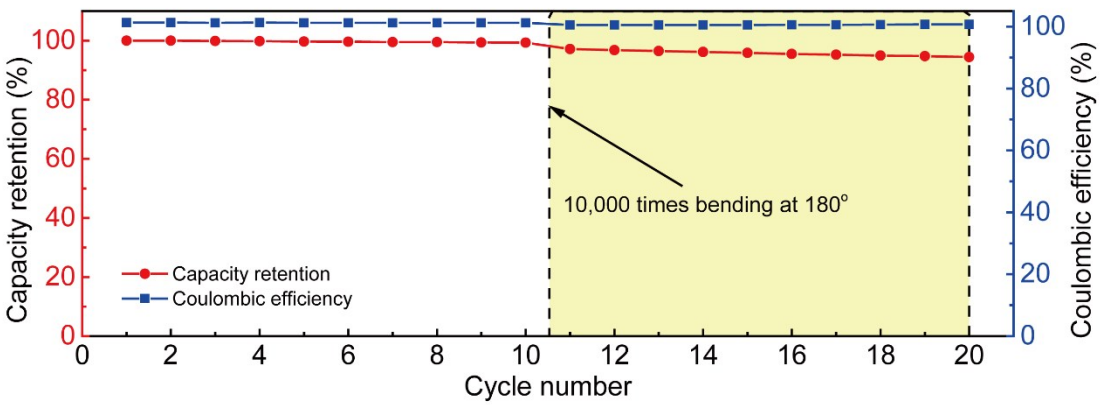

Figure S14. Cyclic stability of the injectable fiber battery before and after 10,000 cycles of bending at a bending angle of 180 ° at current density of 1000 $mA \cdot g^{-1}$.

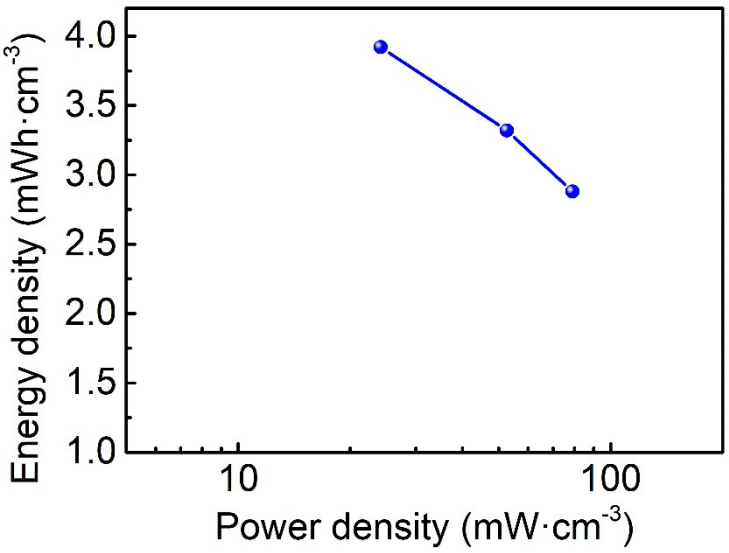

Figure S15. Ragone plot (energy density *versus* power density) of the injectable fiber battery.

Table S1. Comparison of the power density and softness of the injectable fiber battery with currently used batteries in *vivo*.

Category of battery	Power density	Softness	Rechargeability	Reference
Zn/Mg-Cu battery	0.23 $\mu W \cdot mm^{-2}$	Rigid	No	[3]
Mg-MoO_3 battery	0.27 $mW \cdot cm^{-2}$	Rigid	No	[4]
Mg-air battery	3.9 $mW \cdot cm^{-3}$	Rigid	No	[5]
Injectable fiber battery	**78.9 $mW \cdot cm^{-3}$**	**Highly soft**	**100 cycles *in vivo***	**This work**

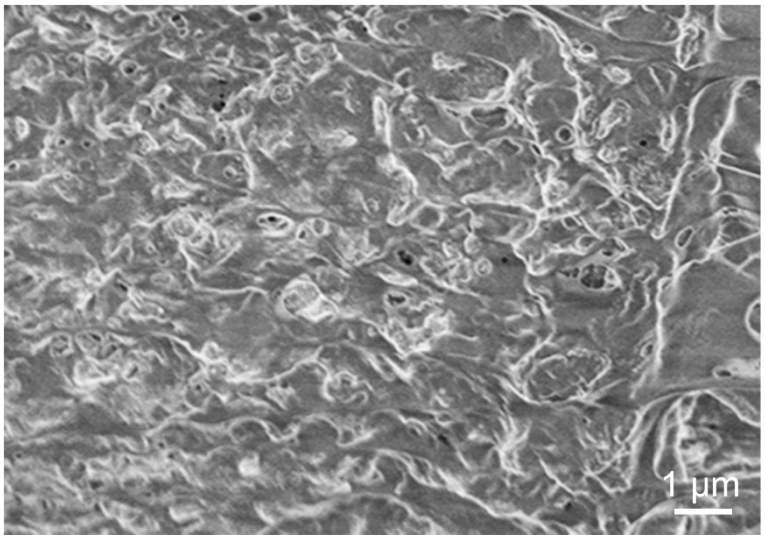

Figure S16. SEM image of the anode hybrid fiber after 100 galvanostatic charge-discharge cycles *in vivo*.

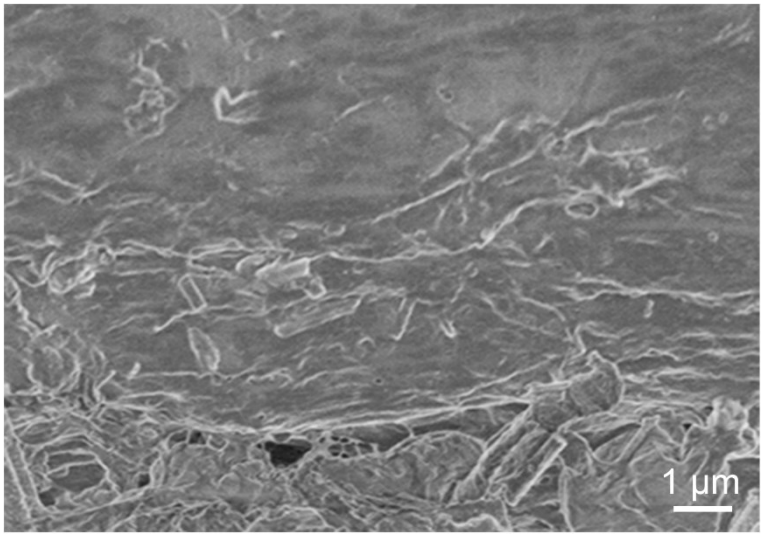

Figure S17. SEM image of the cathode hybrid fiber after 100 galvanostatic charge-discharge cycles *in vivo*.

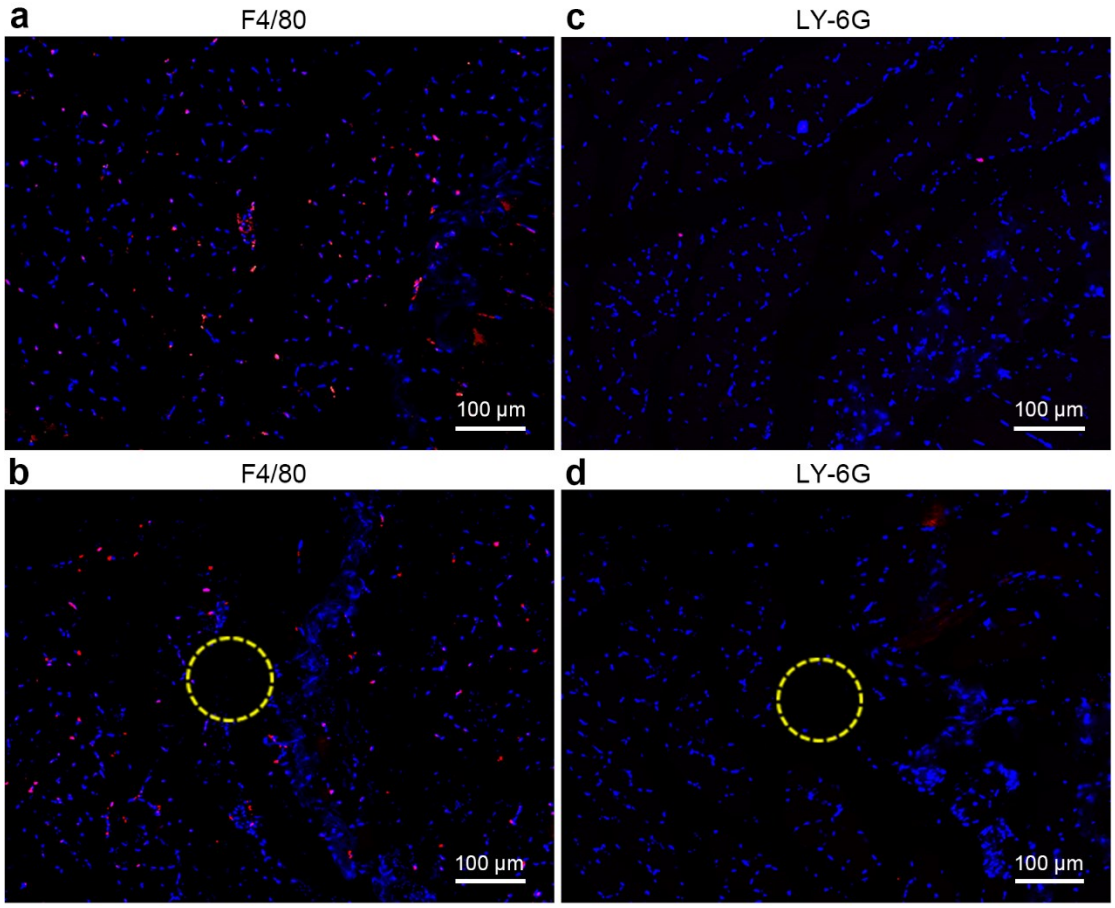

Figure S18. Biocompatibility study of the fiber battery undergoing 100 charge-discharge cycles *in vivo*. a, **b**, F4/80-labelled sections of tissues without and with implanted fiber battery after 30 days, respectively. The nucleus is shown in blue (DAPI) while F4/80 is shown in red. **c**, **d**, LY-6G-labelled sections of tissues without and with implanted fiber battery after 30 days, respectively. The nucleus is shown in blue (DAPI) while LY-6G is shown in red.

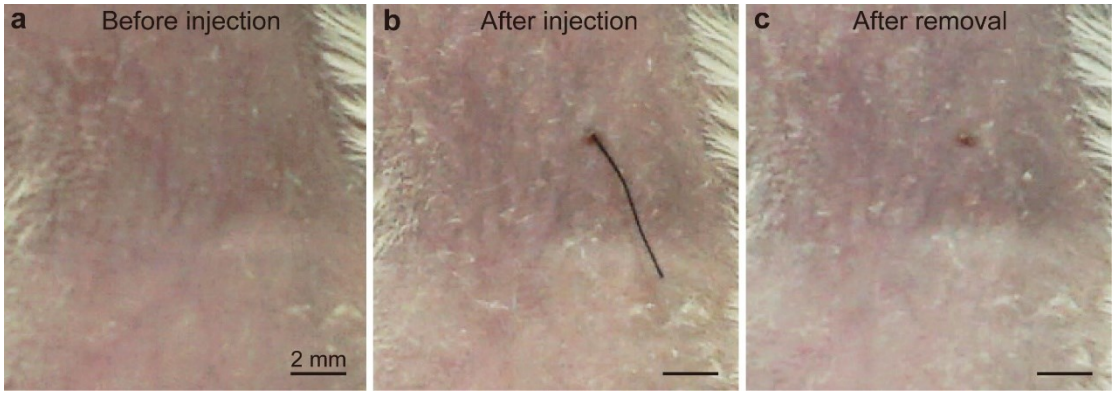

Figure S19. Photographs of the almost non-invasive injection (**a, b**) and removing (**c**) process of the injectable fiber battery.

Supplementary References

1. D. Young, P. Cong, M. Suster and M, Damaser, *Lab Chip*, 2015, **15**, 4338-4347.
2. M. Mimee, P. Nadeau, A. Hayward, S. Carim, S. Flanagan, L. Jerger, J. Collins, S. McDonnell, R. Swartwout, R. Citorik, V. Bulović, R. Langer, G. Traverso, A. Chandrakasan and T. Lu, *Science*, 2018, **360**, 915-918.
3. P. Nadeau, D. El-Damak, D. Glettig, Y. Kong, S. Mo, C. Cleveland, L. Booth, N. Roxhed, R. Langer, A. Chandrakasan and G. Traverso, *Nat. Biomed. Eng.*, 2017, **1**, 0022.
4. X. Huang, D. Wang, Z. Yuan, W. Xie, Y. Wu, R. Li, Y. Zhao, D. Luo, L. Cen, B. Chen, H, Wu, H, Xu, X. Sheng, M, Zhang, L. Zhao and L. Yin, *Small*, 2018, **14**, 1800994.
5. X. Jia, Y. Yang, C. Wang, C. Zhao, R. Vijayaraghavan, D. MacFarlane, M. Forsyth and G. Wallace, *ACS Appl. Mater. Interfaces*, 2014, **6**, 21110-21117.